Available online at www.sciencedirect.com
SCIENCE DIRECT®

Journal of the European Ceramic Society 24 (2004) 2049–2054

www.elsevier.com/locate/jeurceramsoc

Crack growth data from dynamic tests under contact loading?

T. Fett[a,*], D. Creek[b], D. Badenheim[b], R. Oberacker[b]

[a]*Forschungszentrum Karlsruhe, Institut für Materialforschung II, Karlsruhe, 76021, Germany*
[b]*Universität Karlsruhe, Institut für Keramik im Maschinenbau, Karlsruhe, Germany*

Received 16 April 2003; accepted 22 June 2003

Abstract

Bending and contact strength tests at different loading rates were carried out on a commercial alumina. From the comparison of the two strength tests, it was found that the investigated alumina does not exhibit any subcritical crack growth under contact loading, although a strong subcritical crack growth effect is obvious in bending tests. The different behaviour can be explained as the consequence of mode-II failure accompanied with $K_I < 0$ in the contact strength tests and of pure mode-I failure (i.e. $K_I > 0$) in the bending tests.

Keywords: $A1_2O_3$; Crack growth; Test methods

1. Introduction

Different procedures are available to determine the subcritical crack growth behaviour of natural cracks in ceramic materials. One of them is the evaluation of tests under static load. In most cases, these tests are carried out in bending. The most important result of static tests is the exponent n of the subcritical crack growth relation

$$v = \frac{da}{dt} = A\left(\frac{K}{K_{Ic}}\right)^n \tag{1}$$

with K = applied stress intensity factor, K_{Ic} = fracture toughness, and A = the crack growth rate at $K = K_{Ic}$, which is often in the range of $10^{-5}\text{m/s} < A < 10^{-2}\text{m/s}$.

If this exponent is small, the investigated material is very sensitive to subcritical crack growth. For high n-values ($n \to \infty$), no significant subcritical crack growth effect occurs.

For cracks under more homogeneously distributed stresses

$$K = \sigma Y\sqrt{a} \tag{2}$$

is fulfilled.

If the scatter of the inert fracture strength σ_c can be described by the Weibull distribution with the cumulative density function F given by

$$F(\sigma_c) = 1 - \exp[-(\sigma_c/\sigma_0)^m], \tag{3}$$

the consequence of Eqs. (1) and (2) is that also strengths under subcritical crack growth conditions &*sigma*;$_f$ are Weibull-distributed. It results

$$F(\sigma_f) = 1 - \exp\left[-\left(\sigma_f/\sigma_{f0}\right)^{m^*}\right] \tag{4}$$

with

$$m^* = m\frac{n+1}{n-2} \tag{5}$$

for the usually large n-values yielding $m^* \cong m$, and

$$\sigma_{f0} = \left[B\sigma_0^{n-2}\dot{\sigma}(n+1)\right]^{1/(n+1)} \tag{6}$$

The parameter B is related to the crack growth parameters A^* and n by

$$B = \frac{2K_{Ic}^2}{A^* Y^2 (n-2)} \tag{7}$$

with $Y = 1.3$ for semi-circular surface cracks. Plotting the characteristic bending strengths σ_{f0} versus the stress rate $\dot{\sigma}$ in a $\log\sigma_f$–$\log\dot{\sigma}$ diagram yields $1/(1+n)$ as the slope of the regression straight line, from which n is obtained.

* Corresponding author.
E-mail address: theo.fett@imf.fzk.de (T. Fett).

0955-2219/$ - see front matter © 2003 Elsevier Ltd. All rights reserved.
doi:10.1016/S0955-2219(03)00626-5

2. Contact strength tests

Recently, some of the authors developed a contact strength test[1] which needs commonly used bending bars or fragments of already tested specimens only. In this test, mechanical loading leads to strongly non-homogeneous and multiaxial stresses. The test device is shown in Fig. 1. Two cylinders of 8 mm in diameter, made of hardened steel, are pressed onto the rectangular specimen with a force P.

The contact strength σ_f is defined as the maximum tensile stress in the specimen at the moment of failure, which is given by[1]

$$\sigma_f = \sigma_{max} = 0.490\frac{P}{Ht} \tag{8}$$

The contact stresses near the surface cause mixed-mode stress intensity factors for existing surface cracks. Very close to the Hertzian contact zone, $x/s \approx 1$, the formally computed mode-I stress intensity factor is negative as shown in Fig. 2a for edge cracks. Consequently, the effective stress intensity factor represents a pure mode-II loading $K_{II,eff}$ which is equal to the applied stress intensity factor $K_{II,appl}$ reduced by a friction term[2,3] which, in case of the Richard[4] mixed-mode fracture criterion, yields[5]

$$K_{eff} = \sqrt{\tfrac{3}{2}}K_{II,eff},\ K_{II,eff} = K_{II,appl} + \mu K_I \tag{9}$$

with the friction coefficient μ.

As shown in Refs. 2 and 3 and can be concluded from Fig. 2b, the stresses near the end of the Hertzian contact area yield an effective stress intensity factor K_{eff} roughly as

$$K_{eff} = \sigma_{max} Ca \tag{10}$$

Under mixed-mode loading and pure mode-II loading, a crack must extend in a plane deviating from the original one by kinking (Fig. 3a). Following the local stress intensity factor analysis of Cotterell and Rice,[6] the local mixed-mode stress intensity factors k_I and k_{II} can be computed from the effective mode-II stress intensity factor $K_{II,eff}$ acting in the original crack plane. As shown in, Ref.5, it holds

$$k_I = \left[-3\sin\left(\tfrac{1}{2}\beta\right)\cos^2\left(\tfrac{1}{2}\beta\right) - \tfrac{1}{3}\sin^3\left(\tfrac{1}{2}\beta\right)\right]K_{II,eff}(a_0) \tag{11a}$$

$$k_{II} = \left[\cos\left(\tfrac{1}{2}\beta\right)\left(1 - 3\sin^2\left(\tfrac{1}{2}\beta\right)\right) + \tfrac{1}{6}\sin^2\left(\tfrac{4}{5}\beta\right)\right]K_{II,eff}(a_0) \tag{11b}$$

The sudden change of the original direction by an angle β_{kink} results from the condition that the local mode-II stress intensity factor k_{II} in (11b) vanishes. For pure mode-II loading, this leads to a kink angle of $\beta_{kink} \cong -77°$ (Fig. 3b for $K_{II}/K_I \to \infty$). Introducing this value in (11a) yields the actual stress intensity factor

$$k_I = 1.224K_{II,eff} \cong \sqrt{\tfrac{3}{2}}K_{II,eff} = K_{eff} \tag{12}$$

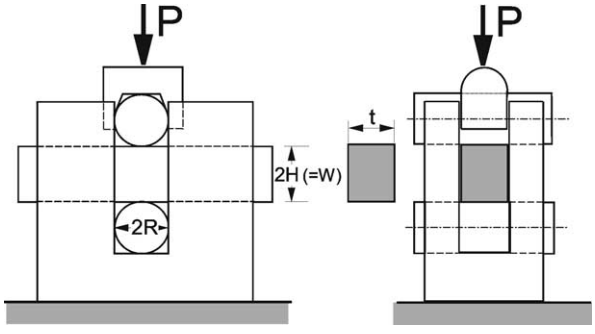

Fig. 1. A two-roller test device for contact strength tests and Hertzian pressure distribution.

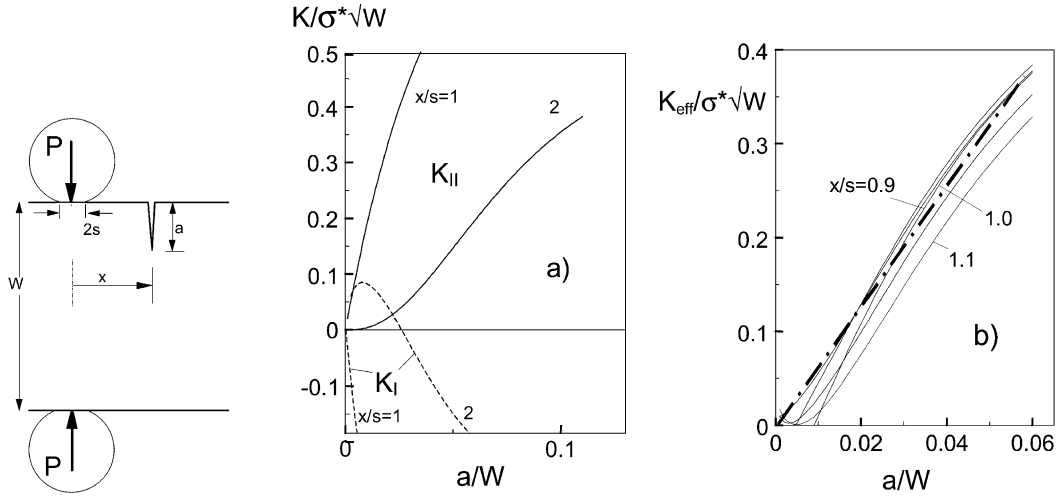

Fig. 2. Stress intensity factors for edge cracks, (a) mode-I and mode-II stress intensity factors for $s/H = 0.1$, (b) effective stress intensity factor according to Eq. (9), computed with $\mu = 0.5$.

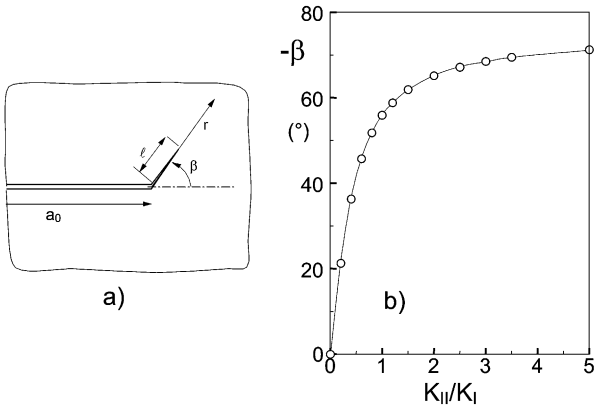

Fig. 3. (a) Kinking crack, (b) kink angle for a crack under mixed-mode loading according to the Richard criterion.[5]

as concluded from Eq. (9). Eq. (12) shows that the stress intensity factor for the kink crack is identical with the effective one and purely mode-I, although a mode-II stress intensity factor is applied.

The considerations of Cotterell and Rice regarding a semi-infinite crack are valid also for finite cracks, if the crack extensions are small compared with the initial crack, i.e. $\ell < a_0$. Fortunately, such small crack extensions are responsible for the main part of the total lifetime. If ℓ is comparable with a_0, we have to replace $K_{\mathrm{eff}}(a_0)$ by

$$K_{\mathrm{eff}}(a) \cong K_{\mathrm{eff}}(a_0 + \ell/\cos\beta) \tag{13}$$

3. Crack growth exponents expected for contact strength tests

The time to failure t_f in a dynamic strength test under contact loading results from Eqs. (1) and (10) as follows

$$\mathrm{d}t = \frac{\mathrm{d}a}{A}\left(\frac{K_{\mathrm{Ic}}}{K}\right)^n = \frac{\mathrm{d}a}{A}\left(\frac{K_{\mathrm{Ic}}}{\sigma_{\max}(t)Ca}\right)^n \tag{14}$$

with $\sigma_{\max}$ given in Eq. (8). Integrating (14) results in

$$\begin{aligned}\int_0^{t_f}\sigma_{\max}^n \mathrm{d}t &= \frac{K_{\mathrm{Ic}}^n}{AC^n}\int_{a_0}^{a_c}\frac{\mathrm{d}a}{a^n} \\ &= \frac{K_{\mathrm{Ic}}^n}{AC^n(n-1)a_0^{n-1}}\left[1-\left(\frac{a_0}{a_c}\right)^{n-1}\right] \\ &\cong \frac{K_{\mathrm{Ic}}^n}{AC^n(n-1)a_0^{n-1}}\end{aligned} \tag{15}$$

Replacing the time increment on the left-hand side of Eq. (14) by the stress increment

$$\mathrm{d}t = \frac{\mathrm{d}\sigma_{\max}}{\dot\sigma_{\max}} \tag{16a}$$

yields

$$\begin{aligned}\int_0^{t_f}\sigma_{\max}^n \mathrm{d}t &= \frac{1}{\dot\sigma_{\max}}\int_0^{\sigma_f}\sigma_{\max}^n \mathrm{d}\sigma_{\max} \\ &= \frac{1}{(n+1)\dot\sigma_{\max}}\sigma_f^{n+1}\end{aligned} \tag{16b}$$

and, consequently,

$$\sigma_{\max}^{n+1} \cong \frac{K_{Ic}^n}{AC^n(n-1)a_0^{n-1}}(n+1)\dot\sigma_{\max} \tag{17}$$

As a consequence of Eq. (10), the initial crack depth can be replaced by the inert contact strength σ_c, i.e. the contact strength in the absence of subcritical crack growth, by

$$K_{\mathrm{Ic}} = Ca_0\sigma_{\mathrm{c}} \tag{18}$$

providing

$$\sigma_{\max}^{n+1} \cong B^*\sigma_c^{n-1}(n+1)\dot\sigma_{\max} \tag{19}$$

with

$$B^* = \frac{K_{\mathrm{Ic}}}{A(n-1)C} \tag{20}$$

Comparing Eq. (19) with Eq. (6) shows that the dynamic contact strength should exhibit the same stress-rate dependency as obtained in dynamic bending tests, namely, a straight line in the $\log\sigma_f$–$\log\dot\sigma$ plot with a slope of $1/(n+1)$.

4. Experimental results

A commercial alumina, Frialit F99.7 (Friatec, Friedrichsfeld), with a median grain size of $d_m \approx 9$ μm was tested. Surface grinding resulted in the roughness parameters: arithmetic surface roughness $R_a = 0.7$ μm, reduced peak height $R_{pk} = 0.3$ μm, core roughness depth $R_k = 1.6$ μm, reduced valley depth $R_{vk} = 1.7$ μm. Fig. 4a shows the Weibull distributions of the 4-point bending strengths for the two extreme loading rates. Characteristic strengths of $\sigma_{f0} = 270$ MPa for $\dot\sigma = 0.007$ MPa/s and 390 MPa for $\dot\sigma = 100$ MPa/s were determined by application of the maximum likelihood procedure.[7] From Eq. (6), a subcritical crack growth exponent of about $n \approx 40$ results. In Fig. 4c the bending strength data are plotted in a $\log\sigma_f$–$\log\dot\sigma$ representation together with data from Ref. 8 obtained for the same material.

The contact strength data obtained for loading rates between 0.04 and 50 MPa/s are given in Fig. 4d. Due to the higher scatter of contact strength data compared with bending strength data[2,3] a larger number of tests under contact loading was necessary to reach a sound judgement of Weibull parameters. The contact strength tests, surprisingly, do not exhibit any subcritical crack growth effect. The characteristic contact strengths σ_{f0} and their 90% confidence intervals are compiled in

Table 1. The related values for the bending tests are given in Table 2. Since the confidence intervals of Table 1 for all stress rates strongly overlap, a significant difference in contact strength at the different loading rates cannot be identified. Consequently, an influence of subcritical crack growth cannot be observed. The results of Fig. 3 again are represented in log σ_f versus log $\dot{\sigma}$ plots in Fig. 4.

5. Discussion

Unexpected, the contact strength tests did not reveal the typical subcritical crack growth effect, an increase in strength with increasing loading rate. The reason may be the special crack opening behaviour for cracks near the Hertzian contact zone, i.e. at $x/s \cong 1$. From Fig. 5a, it can be seen that the (formally calculated) mode-I contribution is negative at this location, denoted as "location 1" in Figs. 5b and 6. The condition $K<0$ ensures that the crack is either totally or partly closed with crack faces in contact in the crack-tip region. Such a crack is illustrated in Fig. 6a. The remaining crack-tip loading parameter is a mode-II stress intensity factor K_{II}, which is influenced by the negative mode-I stress intensity factor contribution which reduces the applied K_{II} via crack surface friction. The effective stress intensity factor K_{eff} is plotted in Fig. 5b and exhibits maximum values near $x/s=1$.

Now let us remember that subcritical crack growth is a environmentally assisted phenomenon. Especially the presence of water at the crack tip reduces the energy for bond breaking and gives rise to crack propagation. Under mode-I loading ($K_I>0$), the crack faces are completely separated and water can follow the crack tip of an advancing crack by diffusion along the crack faces. Under a negative K_I contribution, the contact zone makes diffusion of water to the crack tip impossible. Consequently, water-enhanced subcritical crack growth cannot occur. The rate-independent failure stress under this condition is illustrated in Fig. 6b as the dashed horizontal line.

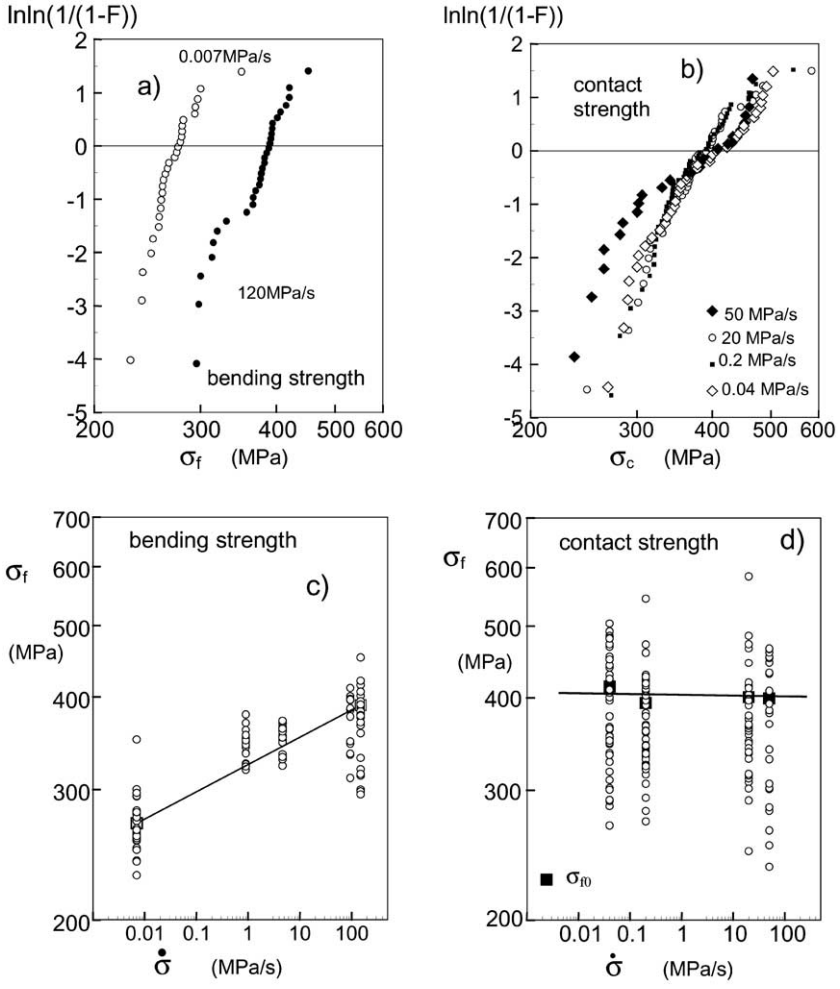

Fig. 4. Dynamic bending strength: (a) and (c) 4-point bending tests, (b) and (d) contact strength tests, squares in (c) and (d): characteristic strength values σ_0.

At location (2), the cracks are open due to the positive mode-I stress intensity factor contribution. Such cracks may extend under normal-water-assisted crack growth conditions. Since the effective stress intensity factor is lower at this location, see Fig. 5b, the inert strength is higher at this location (small effects resulting from different effective surfaces are ignored). This is indicated in Fig. 6b as the horizontal part of the dash-dotted line at high stress rates. These cracks show a stress rate dependency as commonly observed in dynamic bending tests. In Fig. 6b this behaviour is represented by the straight line part with the failure stress decreasing with decreasing stress rate. Finally, the experimentally observable strength behaviour is given as the minimum of the curves for locations (1) and (2).

From the schematic illustration of Fig. 6b, it may be concluded that an influence of $\dot{\sigma}$ may be present at extremely low loading rates. Obviously, the experimental results did not show this effect, i.e. the transition stress rate must be lower than the rates applied in the experiments.

Table 1
Weibull parameters for the contact strengths at different loading rates

$\dot{\sigma}=0.04$ MPa/s	$\sigma_0=414$ [397; 432] MPa	$m=6.9$ [5.3; 7.9]
$\dot{\sigma}=0.2$ MPa/s	$\sigma_0=394$ [379; 409] MPa	$m=6.7$ [5.4; 7.9]
$\dot{\sigma}=20$ MPa/s	$\sigma_0=401$ [383; 419] MPa	$m=6.0$ [4.8; 7.1]
$\dot{\sigma}=50$ MPa/s	$\sigma_0=399$ [373; 427] MPa	$m=5.6$ [4.1; 6.9]

Table 2
Weibull parameters for the bending tests at highest and lowest loading rates

$\dot{\sigma}=0.007$ MPa/s	$\sigma_0=281$ [272; 292] MPa	$m=9.8$ [7.3; 12.0]
$\dot{\sigma}=120$ MPa/s	$\sigma_0=389$ [378; 401] MPa	$m=11.3$ [8.5; 13.8]

6. Conclusions

From the comparison of dynamic bending and dynamic contact strength experiments, it was found that the investigated alumina does not exhibit any subcritical

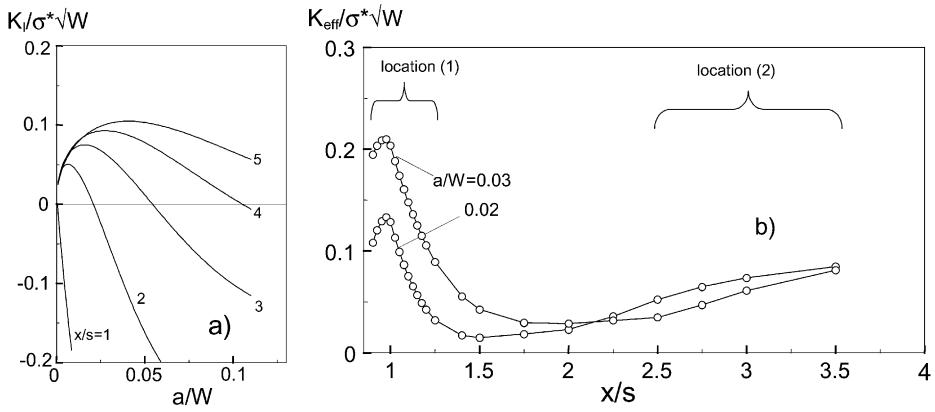

Fig. 5. (a) Mode-I stress intensity factor contribution and (b) effective stress intensity factors for different deep edge cracks at varying distances from the centre of the Hertzian contact zone.

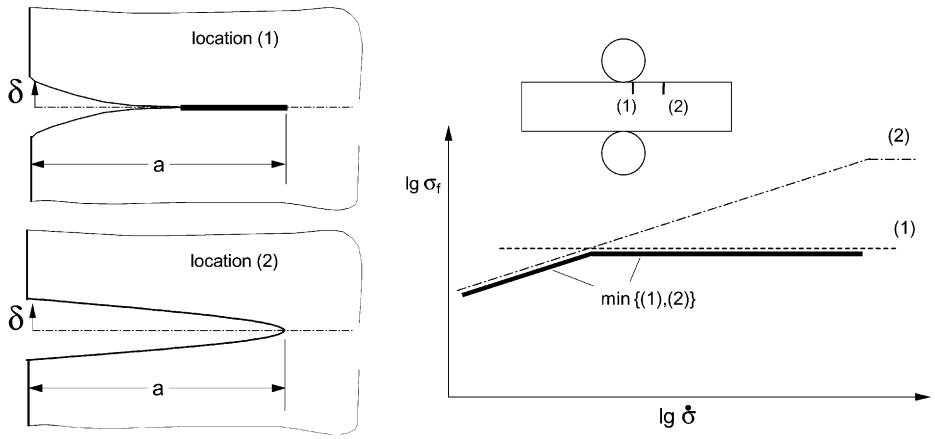

Fig. 6. (a) Crack opening at locations (1) and (2), (b) expected contact strengths under conditions of inhibited subcritical crack growth for $K_I<0$ (1) and normal subcritical crack growth for $K_I>0$ (2).

crack growth under contact loading, although a strong subcritical crack growth effect is obvious in bending tests. Two important consequences may be concluded:

1. Contact strength tests with a variation of the loading rate are no appropriate test for determining the parameters of subcritical crack growth relations.
2. Since the "inert strength" is obtained in all contact strength tests, it is not necessary to perform these tests with extremely high loading rates to obtain the inert contact strength.

Acknowledgements

The authors would like to thank the Deutsche Forschungsgemeinschaft DFG for financing this work within SFB 483.

References

1. Fett, T., Munz, D. and Thun, G., Test devices for strength measurements of bars under contact loading. *Journal of Testing and Evaluation*, 2001, **29**, 1–10.
2. Fett, T. and Munz, D., Influence of stress gradients on failure in contact strength tests with cylinder loading. *Engng. Fract. Mech.*, 2002, **69**, 1353–1361.
3. Fett, T., Ernst, E., Munz, D., Badenheim, D. and Oberacker, R., Effect of multiaxiality and stress gradients on failure in cylinder contact strength tests. *J. Eur. Ceram. Soc.*, 2003, **23**, 2031–2037.
4. Richard, H. A., *Prediction of Fracture of Cracks Subjected to Combined Tensile and Shear Loads* (in German), VDI Research Report 631/85. 1985, Düsseldorf, Germany.
5. Fett, T. and Munz, D., Kinked cracks and Richard fracture criterion. *Int. J. Fracture*, 2002, **115**, L69–L73.
6. Cotterell, B. and Rice, J. R., Slightly curved or kinked cracks. *Int. J. Fracture*, 1980, **16**, 155–169.
7. Thoman, D. R., Bain, L. J. and Antle, C. E., Inferences on the parameters of the Weibull distribution. *Technometrics*, 1969, **11**, 445.
8. Fett, T., Badenheim, D., Oberacker, R., Heiermann, K. and Nejma, R., Subcritical crack growth of Al_2O_3, determined by different methods. *J. Mater. Sci. Lett.*, 2003, **22**, 363–365.